Crystal structure of quizartinib hydrate, $C_{29}H_{32}N_6O_4S\bullet(H_2O)_{1/3}$

James A. Kaduk[1,2], Anja Dosen[3] and Tom N. Blanton[3]
[1]*Department of Chemistry, Illinois Institute of Technology, Chicago, IL 60616, USA*
[2]*Department of Physics, North Central College, Naperville, IL 60540, USA*
[3]*The International Centre for Diffraction Data (ICDD), Newtown Square, PA 19073-3273, USA*

Abstract: The crystal structure of quizartinib hydrate has been solved and refined using synchrotron X-ray powder diffraction data and optimized using density functional theory techniques. Quizartinib hydrate crystallizes in space group *P-1* (#2) with $a = 13.9133(9)$, $b = 17.877(3)$, $c = 19.8459(30)$ Å, $\alpha = 115.080(5)$, $\beta = 93.768(5)$, $\gamma = 100.831(5)°$, $V = 4{,}332.1(6)$ Å^3, and $Z = 6$ at 298 K. In the complex crystal structure, the molecules are generally oriented parallel to the (110) plane. Two of the independent molecules are linked into dimers by N–H···O or N–H···N hydrogen bonds. Each molecule exhibits a unique pattern of C–H···O, C–H···N, or C–H···S hydrogen bonds. The powder pattern has been submitted to ICDD for inclusion in the Powder Diffraction File™ (PDF®).

[doi:10.1017/S0885715625000533]

Key words: quizartinib, Vanflyta®, crystal structure, Rietveld refinement, density functional theory

I. INTRODUCTION

Quizartinib (sold under the brand name Vanflyta®) is used for the treatment of acute myeloid leukemia. It is administered in tablet form and is used in combination with certain chemotherapy medicines and alone as maintenance therapy. The systematic name (CAS Registry No. 950769-58-1) is 1-(5-tert-butyl-1,2-oxazol-3-yl)-3-[4-[6-(2-morpholin-4-ylethoxy)imidazo[2,1-b][1,3]benzothiazol-2-yl]phenyl]urea. A two-dimensional molecular diagram of quizartinib is shown in Figure 1.

X-ray powder diffraction data for Forms A and B of quizartinib, as well as those of a methanol solvate and a hydrochloride salt, are reported in U.S. Patent 8883783B2 (Bhagwat et al. 2014; Ambit Biosciences Corp.). Crystal data for Form B of the hydrochloride salt are also provided, along with powder data for Forms A–O of the hydrochloride and multiple forms of other salts. The powder diffraction pattern of the material reported here does NOT correspond to those of Form A or Form B of quizartinib (Figure 2), nor those of the other solvates or salts.

This work was carried out as part of a project (Kaduk et al. 2014) to determine the crystal structures of large-volume commercial pharmaceuticals and include high-quality powder diffraction data for them in the Powder Diffraction File™ (PDF®; Kabekkodu, Dosen, and Blanton 2024).

II. EXPERIMENTAL

Quizartinib was a commercial reagent, purchased from TargetMol (Batch #T2066), and was used as-received. The white powder was packed into a 0.5-mm-diameter Kapton capillary and rotated during the measurement at ~2 Hz. The powder pattern was measured at 298(1) K at the Wiggler Low Energy Beamline (Leontowich et al. 2021) of the Brockhouse X-ray Diffraction and Scattering Sector of the Canadian Light Source using a wavelength of 0.819563(2) Å (15.1 keV) from 1.6 to 75.0° 2θ with a step size of 0.0025° and a collection time of 3 minutes. The high-resolution powder diffraction data were collected using eight Dectris Mythen2 X series 1K linear strip detectors. NIST SRM 660b LaB_6 was used to calibrate the instrument and refine the monochromatic wavelength used in the experiment.

The pattern was indexed using DICVOL14 (Louër and Boultif 2014) on a primitive triclinic unit cell with $a = 13.936(11)$, $b = 17.939(24)$, $c = 19.899(8)$ Å, $\alpha = 115.24(5)$, $\beta = 93.65(5)$, $\gamma = 100.96(5)$, $V = 4{,}358.57$ Å^3, and $Z = 6$. The space group was assumed to be *P-1*, which was confirmed by the successful solution and refinement of the structure. A reduced cell search of the Cambridge Structural Database (Groom et al. 2016) yielded no hits.

A quizartinib molecule was downloaded from PubChem (Kim et al. 2023) as Conformer3D_COMPOUND_CID_24889293.sdf. It was converted to a *.mol2 file using Mercury (Macrae et al. 2020). The structure was solved by Monte Carlo-simulated annealing techniques, as implemented in EXPO2014 (Altomare et al. 2013), using three molecules as fragments and incorporating a bump penalty. The structure solution contained a void, identified using Mercury with a probe radius of 1.2 Å. An O atom was placed in this void (probably a water molecule). In a preliminary refinement, its position remained constant, and its occupancy refined close to unity. Thus, the compound we studied appears to be a 1/3 hydrate. The hydrogen atoms were added to the water molecule using Materials Studio (Dassault Systèmes 2023), and the structure was optimized using VASP

Corresponding author: James A. Kaduk; Email: kaduk@polycrystallography.com

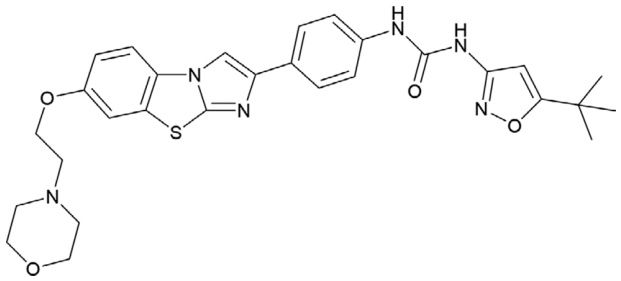

Figure 1. The two-dimensional structure of quizartinib.

(Kresse and Furthmüller 1996) through the MedeA graphical interface (Materials Design, Inc., 2024a).

Rietveld refinement, starting from the VASP-optimized structure, was carried out with GSAS-II (Toby and Von Dreele 2013). Only the 2.0–30.0° portion of the pattern was included in the refinements (d_{min} = 1.583 Å). All non-H-bond distances and angles were subjected to restraints, based on a Mercury/Mogul Geometry Check (Bruno et al. 2004; Sykes et al. 2011). The Mogul average and standard deviation for each quantity were used as the restraint parameters. The imidazobenzthiazol and benzene ring systems were restrained to be planar. The restraints contributed 7.5% to the overall χ^2. There was another void region identified, but placing an O atom there led to a small refined occupancy and movement too close to other atoms, so the atom was removed from the model. The hydrogen atoms were included in calculated positions, which were recalculated during the refinement using Materials Studio (Dassault Systèmes 2023). We did not attempt to refine the displacement coefficients in such a complex structure with limited data. The peak profiles were described by a uniaxial microstrain model, with [100] as the unique axis. A second-order spherical harmonic model was included for the preferred orientation. The background was modeled using a six-term shifted Chebyshev polynomial, with a peak at 11.15° to model the scattering from the Kapton capillary and any amorphous component.

The final refinement of 384 variables using 11,201 observations and 339 restraints yielded the residual R_{wp} = 0.06965. The largest peak (2.01 Å from C178) and hole (1.57 Å from C88) in the difference Fourier map were 0.22(6) and − 0.21 (6) eÅ^{-3}, respectively. The final Rietveld plot is shown in Figure 3. The largest features in the normalized error plot are in the shapes of some of the strong low-angle peaks.

The crystal structure of quizartinib hydrate was optimized (fixed experimental unit cell) with density functional theory techniques using VASP (Kresse and Furthmüller 1996) through the MedeA graphical interface (Materials Design, Inc., 2024a). The calculation was carried out on 32 cores of a 144-core (768-GB memory) HPE Superdome Flex 280 Linux server at North Central College. The calculation used the GGA-PBE functional, a plane wave cutoff energy of 400.0 eV, and a k-point spacing of 0.5 Å^{-1}, leading to a 1 × 1 × 1 mesh, and took ~42 hours. Single-point density functional theory calculations (fixed experimental cell) and population analysis were carried out using CRYSTAL23 (Erba et al. 2023). The basis sets for the H, C, N, and O atoms in the calculation were those of Gatti, Saunders, and Roetti (1994), and that for S was that of Peintinger, Vilela, and Bredow (2013). The calculations were run on a 3.5-GHz PC using 10k-points (SHRINK 3 3) and the B3LYP functional, and took ~18.2 hours.

III. RESULTS AND DISCUSSION

As noted in the Introduction, this material does not correspond to any of the reported forms of quizartinib. It was, however, purchased commercial material, so it may be encountered by others.

The root-mean-square difference of the non-H atoms in the Rietveld-refined and VASP-optimized structures, calculated using the Mercury CSD-Materials/Search/Crystal Packing

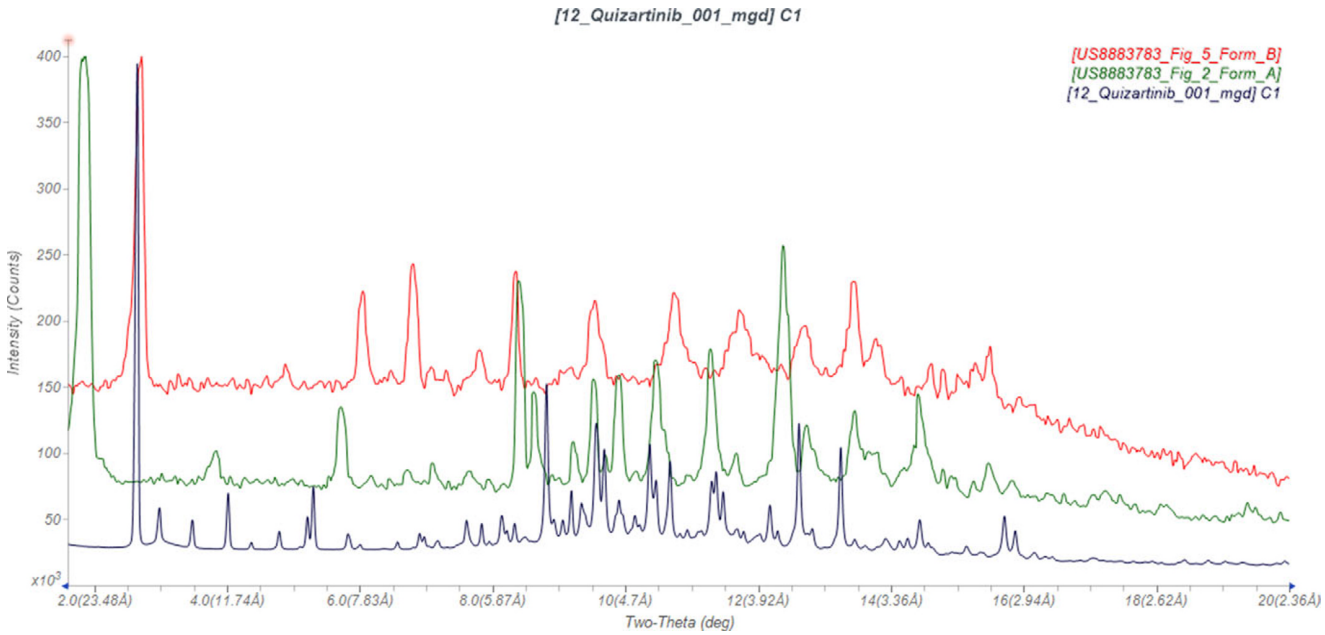

Figure 2. Comparison of the synchrotron pattern of quizartinib (black) to those reported for Forms A and B by Bhagwat et al. (2014) (green and red). The literature patterns (measured using Cu K_α radiation) were digitized using UN-SCAN-IT (Silk Scientific 2013) and converted to the synchrotron wavelength of 0.819563(2) Å using JADE Pro (Materials Design, Inc. [MDI] 2024b). Image generated using JADE Pro (MDI 2024b).

https://doi.org/10.1017/S0885715625000533 Published online by Cambridge University Press

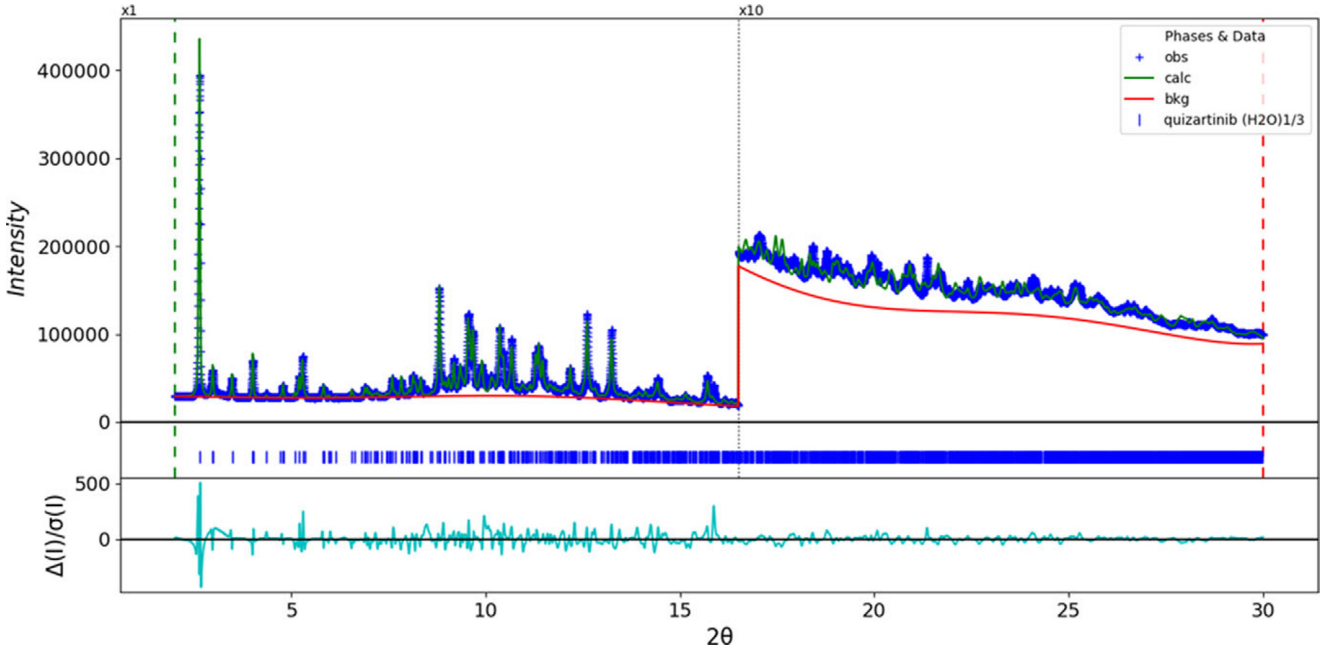

Figure 3. The Rietveld plot for quizartinib hydrate. The blue crosses represent the observed data points, and the green line is the calculated pattern. The cyan curve is the normalized error plot, and the red line is the background curve. The blue tick marks indicate the peak positions. The vertical scale has been multiplied by a factor of 10× for 2θ > 16.5°.

Similarity tool, is 0.358 Å (Figure 4). The root-mean-square Cartesian displacement of the non-H atoms in the Rietveld-refined and VASP-optimized structures of molecules 1–3, calculated using the Mercury Calculate/Molecule Overlay tool, are 0.280, 0.421, and 0.282 Å, respectively (Figures 5–7). The agreements are near the upper end of the normal range for correct structures (van de Streek and Neumann 2014). There is a close contact between O147 and H185 in the refined structure. The asymmetric unit is illustrated in Figure 8. The remaining discussion will emphasize the VASP-optimized structure.

The three independent molecules have different conformations. Molecules 1 and 2 are most similar (rms Cartesian displacement = 1.679 Å, decreasing to 1.385 Å by inverting one of the molecules). Molecules 1 and 3 have an rms displacement of 2.411 Å, and molecules 2 and 3 have an rms displacement of 2.650 Å. Molecules 1 and 2 are more linear in conformation, whereas molecule 3 is kinked.

Most of the bond distances and bond angles fall within the normal ranges indicated by a Mercury Mogul Geometry check (Macrae et al. 2020). The sulfur–carbon bond distances S1–C24, S73–C96, and S145–C168 are flagged as unusual. The optimized values are 1.800–1.801 Å, and the Mogul average is 1.739(20) Å, resulting in *Z*-scores of 3.0. Extended length bonds involving S have been previously reported (Vibha et al. 2023) in VASP-optimized structures, so the calculations may not be as accurate as we might hope. The three equivalent angles C34–C31–C29, C106–C103–C101, and C178–C175–C173 (124.4°; average = 129.6(15)°; *Z*-score = 3.5) are flagged as unusual. Molecules 1–3 have unusual torsion angles involving rotations about 7, 6, and 4 bonds. Most lie on the tails of distributions of similar torsion angles, but rotations about the N10–C40 and N82–C112 bonds in molecules 1 and 2 are truly unusual.

Quantum chemical geometry optimization of isolated quizartinib molecules (DFT/B3LYP/6-31G*/water) using Spartan ‘24 (Wavefunction 2023) indicated that molecule 1 is lowest in energy, and that molecules 2 and 3 are 2.1 and 0.3 kcal/mol higher in energy. Molecules 1 and 2 are about equally similar to the minimum-energy conformation but differ in the orientations of the morpholine/benzothiazole

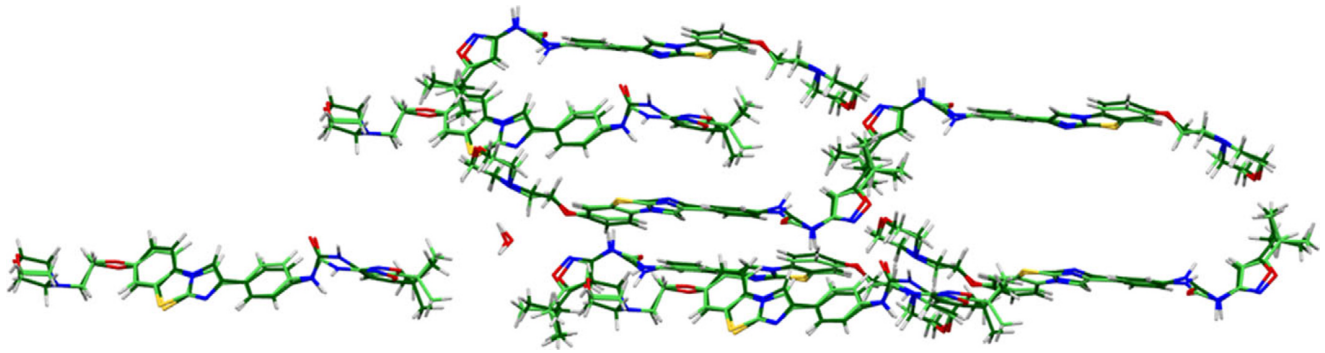

Figure 4. Comparison of the Rietveld-refined (colored by atom type) and VASP-optimized (green) structures of quizartinib hydrate, calculated using the Mercury CSD-Materials/Search/Crystal Packing Similarity tool. The root-mean-square Cartesian displacement is 0.358 Å. Image generated using Mercury (Macrae et al. 2020).

https://doi.org/10.1017/S0885715625000533 Published online by Cambridge University Press

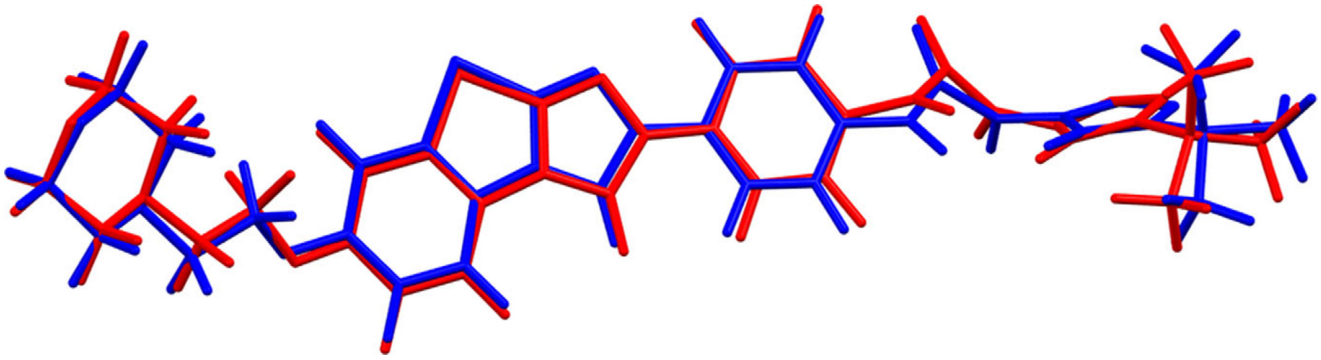

Figure 5. Comparison of the Rietveld-refined (red) and VASP-optimized (blue) structures of molecule 1 in quizartinib hydrate. The root-mean-square Cartesian displacement is 0.280 Å. Image generated using Mercury (Macrae et al. 2020).

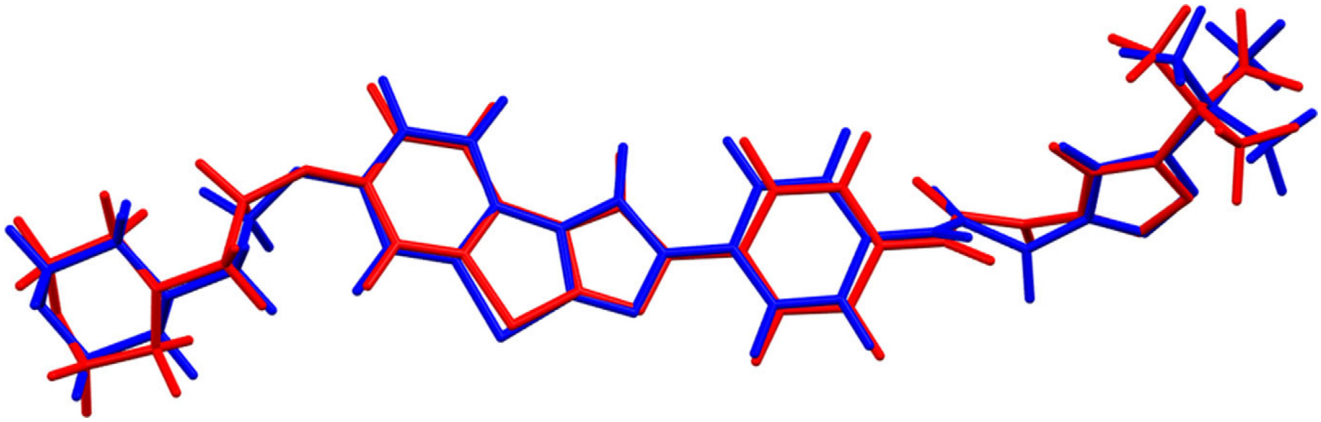

Figure 6. Comparison of the Rietveld-refined (red) and VASP-optimized (blue) structures of molecule 2 in quizartinib hydrate. The root-mean-square Cartesian displacement is 0.421 Å. Image generated using Mercury (Macrae et al. 2020).

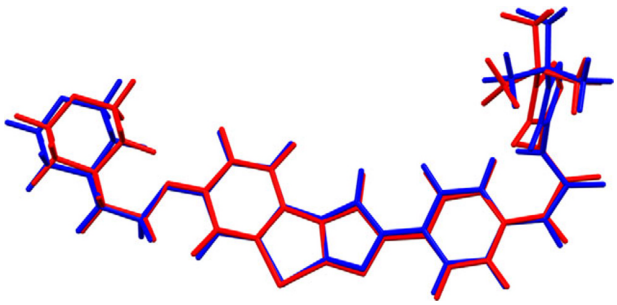

Figure 7. Comparison of the Rietveld-refined (red) and VASP-optimized (blue) structures of molecule 3 in quizartinib hydrate. The root-mean-square Cartesian displacement is 0.282 Å. Image generated using Mercury (Macrae et al. 2020).

and morpholone/oxazole rings, respectively. The minimum-energy conformation is extended, rather than compact (folded on itself). The quizartinib molecule is apparently very flexible, as large conformational changes result in small differences in energy. Presumably, intermolecular interactions are important in determining the observed solid-state conformations.

The complex crystal structure (Figure 9) is hard to describe succinctly. The molecules are positioned in quasi-parallel layers along the (110) plane. The actual layers are hard to see, and our best depiction is shown in Figure 9. The mean planes of the molecules are approximately (6, 8, −1), (2, 1, −1), and (6, 5, 5). The Mercury Aromatics Analyser indicates one moderate interaction between molecules 1 and 2, with a distance of 4.75 Å.

Analysis of the contributions to the total crystal energy of the structure using the Forcite module of Materials Studio (Dassault Systèmes 2023) indicates that the intramolecular energy is dominated by angle distortion terms, as might be expected for a molecule containing a fused ring system. The intermolecular energy is dominated by electrostatic attractions, which, in this force field-based analysis, also include hydrogen bonds. The hydrogen bonds are better discussed using the results of the DFT calculation.

There are perhaps not as many hydrogen bonds in the structure as anticipated (Table I). The water molecule makes a strong O217–H218···N8 hydrogen bond to the ring N atom N8. It makes a much weaker O217–H219···N155 to the amino group N155. The amino group N10 makes a strong N10–H69···O5 hydrogen bond to the carbonyl group O5 of an adjacent molecule 1. This links two molecule 1 units into dimers, with a graph set *R2,2(8)* (Bernstein et al. 1995; Etter 1990; Motherwell, Shields, and Allen 2000). The comparable amino group N82 in molecule 2 forms only a weak N–H···N hydrogen bond to the ring atom N8 in molecule 1. The equivalent amino group N154 in molecule 3 forms a strong N–H···N hydrogen bond to the ring N153 in adjacent molecule 3, linking them into dimers with a graph set *R2,2(8)*. Each molecule exhibits a unique pattern of C–H···O, C–H···N, or C–H···S hydrogen bonds.

https://doi.org/10.1017/S0885715625000533 Published online by Cambridge University Press

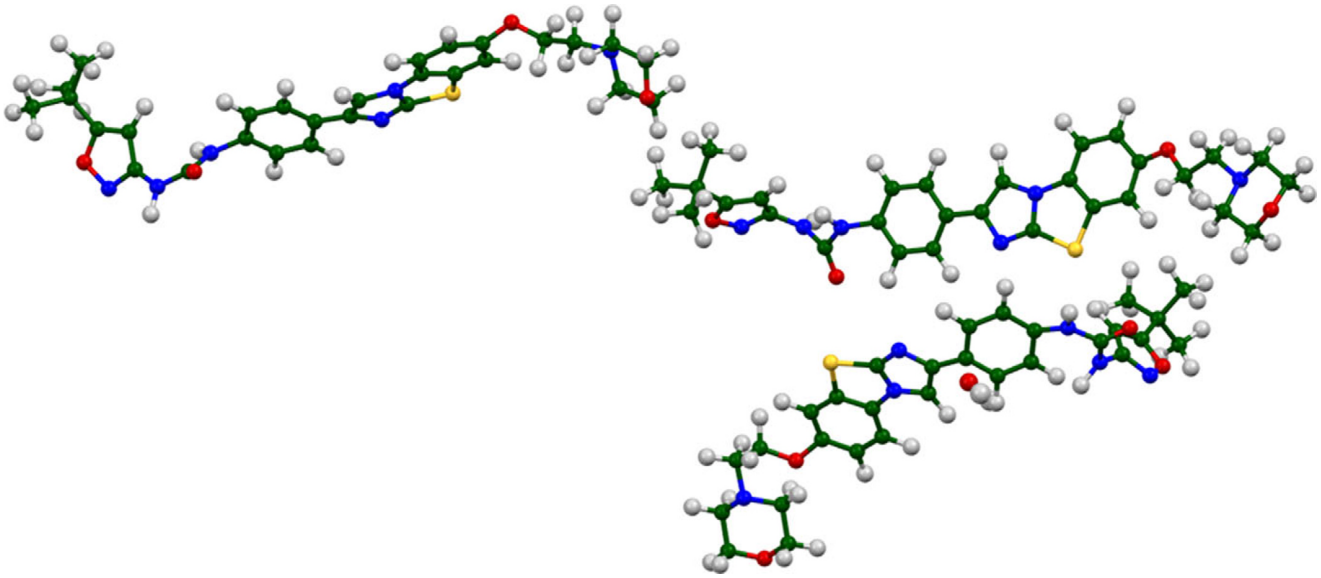

Figure 8. The asymmetric unit of quizartinib hydrate. This ball-and-stick image was generated using Mercury (Macrae et al. 2020).

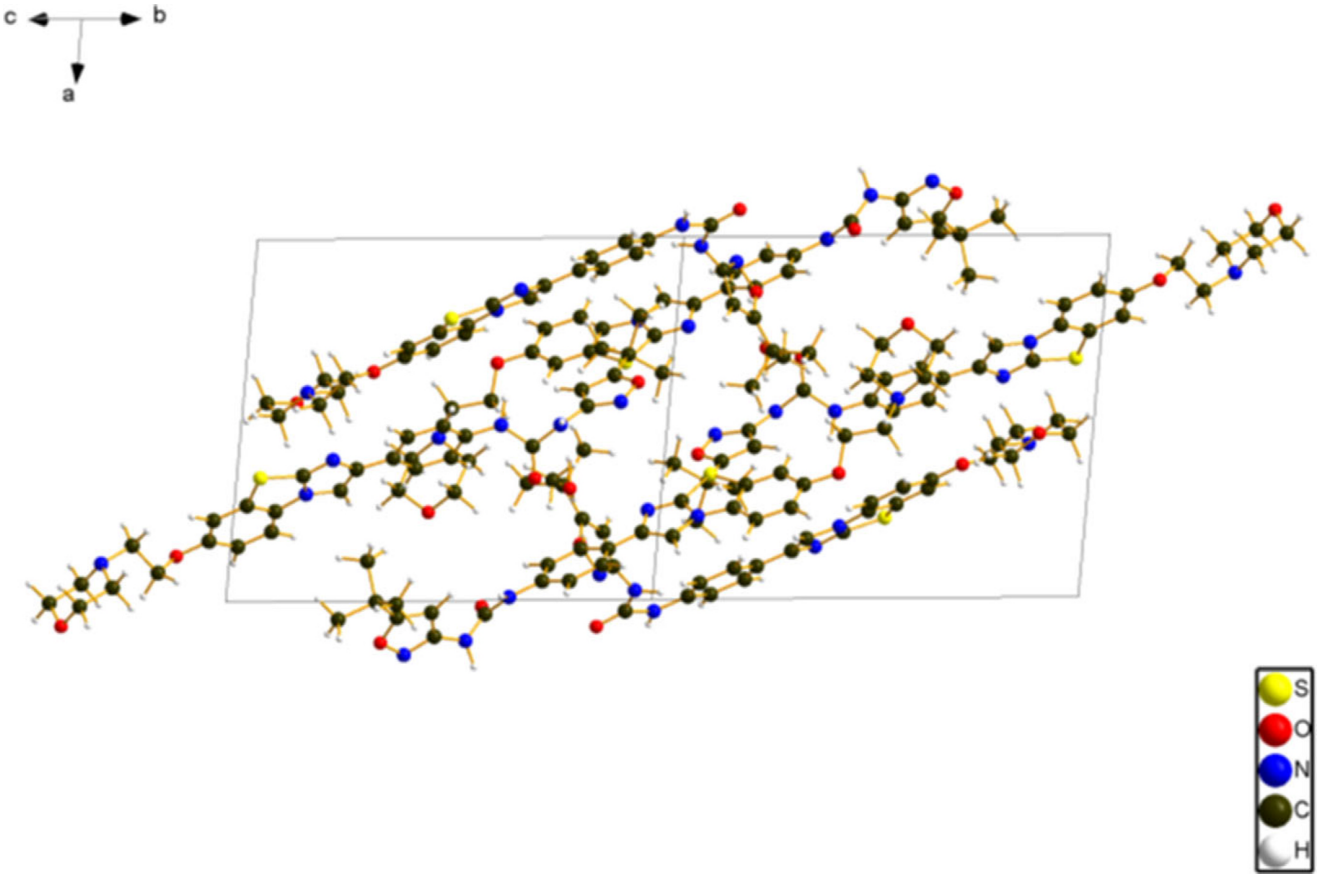

Figure 9. The crystal structure of quizartinib hydrate, viewed down [011]. Image generated using Diamond (Crystal Impact 2023).

The volume enclosed by the Hirshfeld surface of quizartinib hydrate (Figure 10; Hirshfeld 1977; Spackman et al. 2021) is 2,145.94 Å^3, 99.07% of 1/2 of the unit cell volume. The packing density is thus fairly dense. The only significant close contacts (red in Figure 10) involve the hydrogen bonds. Fingerprint plots indicate that H···H contacts make up 56.5% of the surface area. The volume/non-hydrogen atom is typical at 17.6 Å^3.

The Bravais–Friedel–Donnay–Harker (Bravais 1866; Donnay and Harker 1937; Friedel 1907) algorithm suggests that we should expect slightly elongated morphology for quizartinib hydrate, with [100] as the long axis. A second-order spherical

https://doi.org/10.1017/S0885715625000533 Published online by Cambridge University Press

TABLE I. Hydrogen bonds (CRYSTAL23) in quizartinib hydrate

H bond	D–H, Å	H···A, Å	D···A, Å	D–H···A, °	Mulliken overlap (*e*)
O217–H218···N8	0.990	1.960	2.950	179.6	0.049
O217–H219···H155	0.974	2.513	3.307	138.6	0.010
N10–H69···O5	1.044	1.746	2.777	168.2	0.070
N82–H141···N8	1.019	2.895	3.765	143.8	0.010
N154–H213···N153	1.044	1.812	2.849	171.5	0.083
C15–H47···N78	1.102	2.359	3.457	174.3	0.032
C20–H53···O74	1.098	2.254	3.330	166.1	0.028
C92–H126···O149	1.100	2.604	3.684	167.1	0.015
C39–H71···O5	1.083	2.069*	2.782	119.0	0.018
C84–H113···O147	1.099	2.539	3.577	157.2	0.011
C93–H130···O217	1.098	2.687	3.334	117.1	0.011
C94–H133···S1	1.099	2.979	3.793	131.1	0.017
C107–H139···N80	1.088	2.484*	2.852	98.5	0.014
C108–H140···N9	1.091	2.478	3.358	136.9	0.017
C180–H212···N152	1.088	2.655*	2.976	96.2	0.010
C171–H206···O77	1.089	2.365	3.288	141.4	0.018
C172–H207···O2	1.091	2.879	3.751	137.0	0.012
C182–H214···N153	1.085	2.364	3.385	156.1	0.011

*Intramolecular.

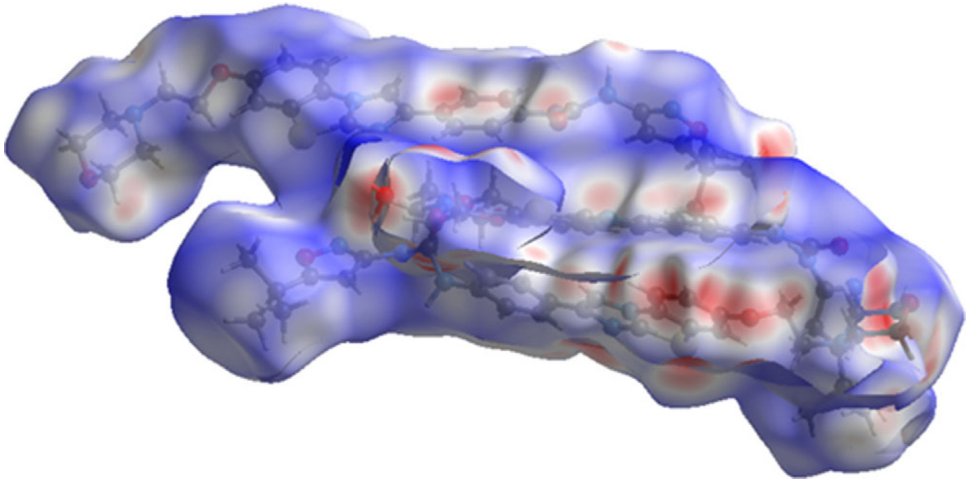

Figure 10. The Hirshfeld surface of quizartinib hydrate. Intermolecular contacts longer than the sum of the van der Waals radii are colored blue, and contacts shorter than the sum of the radii are colored red. Contacts equal to the sum of the radii are white. Image generated using CrystalExplorer (Spackman et al. 2021).

harmonic model was included in the refinement. The texture index was 1.057(3), indicating that the preferred orientation was slight in this rotated capillary specimen.

DEPOSITED DATA

The powder pattern of quizartinib hydrate from this synchrotron data set has been submitted to ICDD for inclusion in PDF. The Crystallographic Information Framework (CIF) files containing the results of the Rietveld refinement (including the raw data) and the DFT geometry optimization were deposited with the ICDD. The data can be requested at pdj@icdd.com.

ACKNOWLEDGEMENTS

We thank Adam Leontowich for his assistance in the data collection. We also thank the ICDD team – Megan Rost, Steve Trimble, and Dave Bohnenberger – for their contribution to research, sample preparation, and in-house XRD data collection and verification.

FUNDING STATEMENT

Part or all of the research described in this paper was performed at the Canadian Light Source, a national research facility of the University of Saskatchewan, which is supported by the Canada Foundation for Innovation (CFI), the Natural Sciences and Engineering Research Council (NSERC), the Canadian Institute of Health Research (CIHR), the Government of Saskatchewan, and the University of Saskatchewan. This work was partially supported by the International Centre for Diffraction Data.

CONFLICTS OF INTEREST

The authors have no conflicts of interest to declare.

https://doi.org/10.1017/S0885715625000533 Published online by Cambridge University Press

REFERENCES

Altomare, A., C. Cuocci, C. Giacovazzo, A. Moliterni, R. Rizzi, N. Corriero, and A. Falcicchio. 2013. "EXPO2013: A Kit of Tools for Phasing Crystal Structures from Powder Data." *Journal of Applied Crystallography* 46: 1231–5.

Bernstein, J., R. E. Davis, L. Shimoni, and N. L. Chang. 1995. "Patterns in Hydrogen Bonding: Functionality and Graph Set Analysis in C." *Angewandte Chemie International Edition in English* 34: 1555–73.

Bhagwat, S. S., W. Lai, S. D. Parent, M. J. Roe, A. Schwartz, and V. N. Smolenskaya. 2014. "Solid Forms Comprising N-(5-tert-butyl-isoxazol-3-yl)-N'-{4-[7-(2-morpholin-4-yl-ethoxy)imidazo[2,1-B][1,3]benzothiazol-2-yl]phenyl]urea, Compositions Thereof, and Uses Therewith." U.S. Patent 8883783B2.

Bravais, A. 1866. *Etudes Cristallographiques*. Paris: Gauthier Villars.

Bruno, I. J., J. C. Cole, M. Kessler, J. Luo, W. D. S. Motherwell, L. H. Purkis, B. R. Smith, et al. 2004. "Retrieval of Crystallographically-Derived Molecular Geometry Information." *Journal of Chemical Information and Computer Sciences* 44: 2133–44.

Crystal Impact. 2023. *Diamond V. 5.0.0*. Bonn: Crystal Impact (Dr. H. Putz & Dr. K. Brandenburg).

Dassault Systèmes. 2023. *BIOVIA Materials Studio 2024*. San Diego, CA: BIOVIA.

Donnay, J. D. H., and D. Harker. 1937. "A New Law of Crystal Morphology Extending the Law of Bravais." *American Mineralogist* 22: 446–67.

Erba, A., J. K. Desmarais, S. Casassa, B. Civalleri, L. Donà, I. J. Bush, B. Searle, et al. 2023. "CRYSTAL23: A Program for Computational Solid State Physics and Chemistry." *Journal of Chemical Theory and Computation* 19: 6891–932. https://doi.org/10.1021/acs.jctc.2c00958

Etter, M. C. 1990. "Encoding and Decoding Hydrogen-Bond Patterns of Organic Compounds." *Accounts of Chemical Research* 23: 120–6.

Friedel, G. 1907. "Etudes sur la loi de Bravais." *Bulletin de la Société Française de Minéralogie* 30: 326–455.

Gatti, C., V. R. Saunders, and C. Roetti. 1994. "Crystal-Field Effects on the Topological Properties of the Electron-Density in Molecular Crystals – The Case of Urea." *Journal of Chemical Physics* 101: 10686–96.

Groom, C. R., I. J. Bruno, M. P. Lightfoot, and S. C. Ward. 2016. "The Cambridge Structural Database." *Acta Crystallographica Section B: Structural Science, Crystal Engineering and Materials* 72: 171–79.

Hirshfeld, F. L. 1977. "Bonded-Atom Fragments for Describing Molecular Charge Densities." *Theoretica Chemica Acta* 44: 129–38.

Kabekkodu, S., A. Dosen, and T. N. Blanton. 2024. "PDF-5+: A Comprehensive Powder Diffraction File™ for Materials Characterization." *Powder Diffraction* 39: 47–59.

Kaduk, J. A., C. E. Crowder, K. Zhong, T. G. Fawcett, and M. R. Suchomel. 2014. "Crystal Structure of Atomoxetine Hydrochloride (Strattera), $C_{17}H_{22}NOCl$." *Powder Diffraction* 29: 269–73.

Kim S., J. Chen, T. Cheng, A. Gindulyte, J. He, S. He, Q. Li, et al. 2023. "PubChem 2023 Update." *Nucleic Acids Research* 51 (D1): D1373–80. https://doi.org/10.1093/nar/gkac956

Kresse, G., and J. Furthmüller. 1996. "Efficiency of Ab-Initio Total Energy Calculations for Metals and Semiconductors Using a Plane-Wave Basis Set." *Computational Materials Science* 6: 15–50.

Leontowich, A. F. G., A. Gomez, B. Diaz Moreno, D. Muir, D. Spasyuk, G. King, J. W. Reid, C.-Y. Kim, and S. Kycia. 2021. "The Lower Energy Diffraction and Scattering Side-Bounce Beamline for Materials Science at the Canadian Light Source." *Journal of Synchrotron Radiation* 28: 1–9. https://doi.org/10.1107/S1600577521002496

Louër, D., and A. Boultif. 2014. "Some Further Considerations in Powder Diffraction Pattern Indexing with the Dichotomy Method." *Powder Diffraction* 29: S7–12.

Macrae, C. F., I. Sovago, S. J. Cottrell, P. T. A. Galek, P. McCabe, E. Pidcock, M. Platings, et al. 2020. "*Mercury 4.0*: From Visualization to Design and Prediction." *Journal of Applied Crystallography* 53: 226–35.

Materials Design, Inc. 2024a. *MedeA 3.7.2*. San Diego, CA: Materials Design, Inc.

Materials Design, Inc. 2024b. *JADE Pro Version 9.0*. Livermore, CA: Materials Data, Inc.

Motherwell, W. D. S., G. P. Shields, and F. H. Allen. 2000. "Graph-Set and Packing Analysis of Hydrogen-Bonded Networks in Polyamide Structures in the Cambridge Structural Database." *Acta Crystallographica B* 56: 857–71.

Peintinger, M. F., D. Vilela Oliveira, and T. Bredow. 2013. "Consistent Gaussian Basis Sets of Triple-Zeta Valence with Polarization Quality for Solid-State Calculations." *Journal of Computational Chemistry* 34: 451–9.

Silk Scientific Corporation. 2013. *UN-SCAN-IT 7.0*. Orem, UT: Silk Scientific Corporation.

Spackman, P. R., M. J. Turner, J. J. McKinnon, S. K. Wolff, D. J. Grimwood, D. Jayatilaka, and M. A. Spackman. 2021. "CrystalExplorer: A Program for Hirshfeld Surface Analysis, Visualization and Quantitative Analysis of Molecular Crystals." *Journal of Applied Crystallography* 54: 1006–11. https://doi.org/10.1107/S1600576721002910; https://crystalexplorer.net

Sykes, R. A., P. McCabe, F. H. Allen, G. M. Battle, I. J. Bruno, and P. A. Wood. 2011. "New Software for Statistical Analysis of Cambridge Structural Database Data." *Journal of Applied Crystallography* 44: 882–6.

Toby, B. H., and R. B. Von Dreele. 2013. "GSAS II: The Genesis of a Modern Open Source All Purpose Crystallography Software Package." *Journal of Applied Crystallography* 46: 544–9.

van de Streek, J., and M. A. Neumann. 2014. "Validation of Molecular Crystal Structures from Powder Diffraction Data with Dispersion-Corrected Density Functional Theory (DFT-D)." *Acta Crystallographica Section B: Structural Science, Crystal Engineering and Materials* 70: 1020–32.

Vibha, K., N. C. Prachality, R. A. Reddy, M. N. Ravikantha, and J. Thipperudrappa. 2023. "Computational Studies on Sulfonamide Drug Molecules by Density Functional Theory." *Chemical Physics Impact* 6: 100147. https://doi.org/10.1016/j.chphi.2022.100147

Wavefunction, Inc. 2023. *Spartan '24. V. 1.0.0*. Irvine CA: Wavefunction Inc.

https://doi.org/10.1017/S0885715625000533 Published online by Cambridge University Press